29th International Cosmic Ray Conference Pune (2005) **10**, 97–114

H.E.S.S. Highlights

W. Hofmann for the H.E.S.S. Collaboration
Max-Planck-Institut für Kernphysik, Heidelberg
Presenter: Werner Hofmann (werner.hofmann@mpi-hd.mpg.de)

H.E.S.S. has been in full operation since December 2003 and has provided a wealth of exciting new results from the survey of the Galactic plane at VHE energies, and on VHE gamma-ray emission from supernova remnants, binary systems and pulsar wind nebulae. New results are also reported for Galactic center sources and for distant extragalactic sources, the latter implying novel constraints on the level of extragalactic background light.

1. The H.E.S.S. telescope system

H.E.S.S. is a system of four large (13 m diameter) imaging atmospheric Cherenkov telescopes (Fig. 1), operated by an international collaboration of about 100 physicists from 8 countries. The telescopes [1] are located

Figure 1. The H.E.S.S. telescope system

in the Khomas highland of Namibia, near the tropic of Capricorn. With their cameras [2] containing 960 photomultiplier pixels and covering a 5° field of view, they provide multiple images of gamma-ray (and cosmic-ray) induced air showers in the Cherenkov light emitted by the shower particles, and enable the stereoscopic reconstruction of the shower geometry as well as, from the observed intensity and the reconstructed distance between telescopes and shower axis, the determination of the shower energy. The full four-telescope system is in operation since December 2003, and was officially inaugurated by the Namibian Prime Minister in September 2004. The telescopes operate about 1000 h per year during moonless night time, recording shower events at a rate of about 300 Hz. Near zenith, the energy threshold - defined as the energy of peak detection rate for typical source spectra - is about 100 GeV, increasing with zenith angle to 250 GeV at 45° and 700 GeV at 60°. The system provides an angular resolution of 0.1° for individual gamma-rays; gamma-ray sources can typically be located with a precision of 1' or better, limited for intense sources by systematic errors at the 20" level. The sensitivity of the H.E.S.S. telescope system is about one order of magnitude better than previous instruments, and allows to detect sources with a flux of 1% of the Crab Nebula in 25 h of observations.

Highlights from H.E.S.S. include the Galactic plane survey, which unveiled a large number of new VHE gamma-ray sources, the detailed studies of supernova remnants and pulsar wind nebulae, the discovery of

gamma rays from binary systems and the study of emission from the Galactic center region. While the location of H.E.S.S. in the southern hemisphere emphasizes Galactic sources, exciting results have also been obtained for extragalactic objects.

Lack of space prevents coverage of all results and the in-depth discussion of the numerous sources; for details and further references, the reader is referred to the H.E.S.S. publications cited, and to the other H.E.S.S. contributions in these proceedings. Part of the material presented here is taken from a write-up of a presentation at the Cherenkov 2005 conference [3]. Unpublished results should be considered preliminary.

2. The H.E.S.S. Galactic plane survey

The H.E.S.S. Galactic plane survey (Fig. 2) was

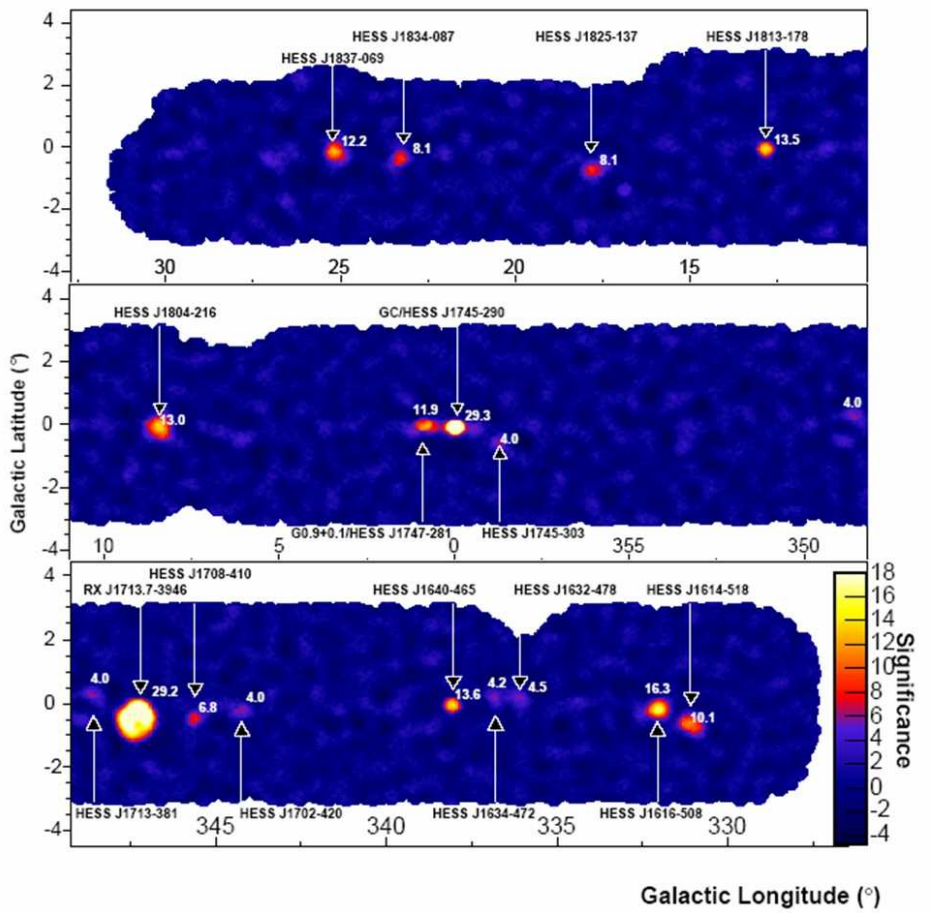

Figure 2. Significance map for the H.E.S.S. survey of the central section of the Galactic plane. Gamma-ray sources are indicated with their HESS J name and (post-trials) significance. The typical energy threshold for this map is 250 GeV. The on-source counts for each coordinate point are integrated over a radius of 0.22°, optimized for slightly extended sources.

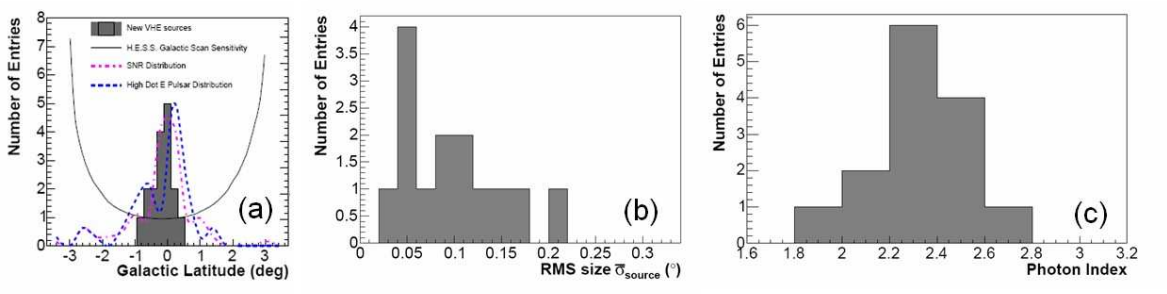

Figure 3. (a) Distribution in Galactic latitude of the sources detected in the survey. The mean of the distribution is -0.17° with an rms of 0.31°. For comparison, the latitude distribution of supernova remnants and of pulsars with high spin-down luminosity is included (red and blue dashed lines, respectively). (b) Distribution of the rms angular size of the new sources. (c) Distribution of the photon index of the new sources. The mean index is 2.3 with an rms of 0.2.

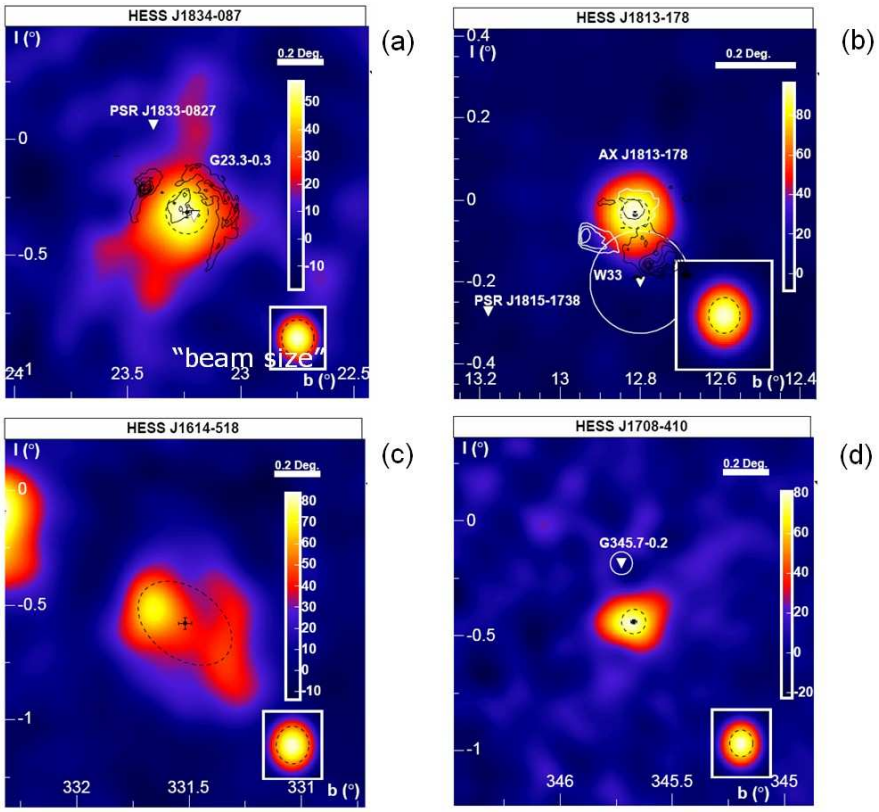

Figure 4. Smoothed excess maps of some of the new sources, together with potential counterparts in other wavelength ranges. The small inset shows the point spread function after smoothing. (a) HESS J1834-087, coincident with SNR G23.3-0.3 (W41); black contours show the radio emission [8]. (b) HESS J1813-178, with radio contours (black) and ASCA X-ray contours (white). (c) HESS J1614-518 and (d) HESS J1708-410; for either source no counterpart is known.

conducted in the summer of 2004 and covered the region of $\pm 30^\circ$ in Galactic longitude and $\pm 3^\circ$ in latitude, at a typical sensitivity of a few % of the Crab flux. In total, 15 new VHE gamma ray sources were discovered during the survey, in addition to three previously known sources in the survey region - the Galactic center, G0.9+0.1, and RX J1713.7-3946. The eight strongest sources, with a post-trial significance exceeding 6σ, were published in [4]; a detailed account of 14 sources, including 6 fainter ones, is given in [5, 6]. In addition, the discovery of a source coincident with the microquasar LS 5039 was presented separately in [7]. The sources line up along the Galactic equator (Fig. 3(a)), with a rms spread in latitude of 0.3°, consistent with the scale height of the distribution of molecular gas and with the width of the distribution of supernova remnants and pulsars. Their Galactic origin is confirmed by the fact that nearly all sources are extended, with rms sizes up to 0.2° (Fig. 3(b)). H.E.S.S. can typically resolve a source as extended when its rms size exceeds 2'-3'. For all new sources, energy spectra could be determined [5]; photon indices range from 1.8 to 2.7 (Fig. 3(c)), with a mean of 2.3, roughly consistent with the expectation for shock wave acceleration of charged particles.

Counterparts for the new sources were searched, primarily in radio- and X-ray catalogs. Five sources could be related to supernova remnants; one example is HESS J1834-087, which nicely coincides with the shell SNR G23.3-0.3 (Fig. 4(a)).

A few of the new sources might be associated with pulsar wind nebulae, although the VHE emission is often offset from the pulsar location – this will be discussed later in more detail. Some of the new sources coincide with EGRET or ASCA unidentified sources. At least three have no counterpart known to us and are sometimes termed "Dark accelerators". However, one of the sources which remained unidentified in the original survey paper [4] – HESS J1813-178 – has meanwhile been identified; it coincides with a supernova ring discovered in radio data [9, 10], and also with previously unpublished ASCA [11] and INTEGRAL [11] sources (Fig. 4(b)). Other unidentified H.E.S.S. sources include HESS J1614-518 and HESS J1708-410 (Fig. 4(c,d)).

3. Supernova remnants studied with H.E.S.S.

Another H.E.S.S. highlight is the detection of resolved supernova remnant (SNR) shells (Fig. 5), for RX J1713.7-3946 [12, 13] and for RX J0852.0-4622 ("Vela Junior") [14, 15], both objects discovered in VHE gamma-rays by CANGAROO [16, 17]. In both cases, TeV gamma ray emission can be clearly traced to the supernova shell, demonstrating that the shock wave accelerates particles to multi-TeV energies, generating photons via interactions with gas – in case of protons - or by Inverse Compton scattering – in case of accelerated electrons. While the intensity of the gamma-ray emission varies along the circumference, the strong correlation with the location of the shell - as seen e.g. in X-rays - is evident. The energy spectrum of RX 1713.7-3964 has been measured over two decades in energy (Fig. 6(a)), up to 30 TeV, and approximately follows a power law with index 2.1 to 2.3, with indications for a cutoff or break at the highest energies. The spectral index coincides with predictions of shock-wave acceleration models; the high photon energies which are detected show that energies of primary particles reach up to 10^{14} eV and beyond. The spectral index is - within errors - constant across the entire remnant (Fig. 6(b)).

To probe the emission mechanisms, it is instructive to look at intensities along two orthogonal slices across RX J1713.7-3946 (Fig. 7). One slice goes from the high-intensity region to the low-intensity region (top row of images), the other (bottom row) in the orthogonal direction. The top gamma-ray slice (left) shows variations in intensity by a factor 3-4; the distribution of gamma rays matches closely the distribution of X-rays [18] (middle), as would be expected for a population of primary electrons. For a proton accelerator, one would expect the gamma-ray intensity to correlate with gas density as measured by the CO emission [20] (right); while a certain correlation is visible, it is not nearly as striking as in the case of X-rays. However, the comparison with the CO emission as a measure of gas density suffers from the limited depth information. Despite a rough

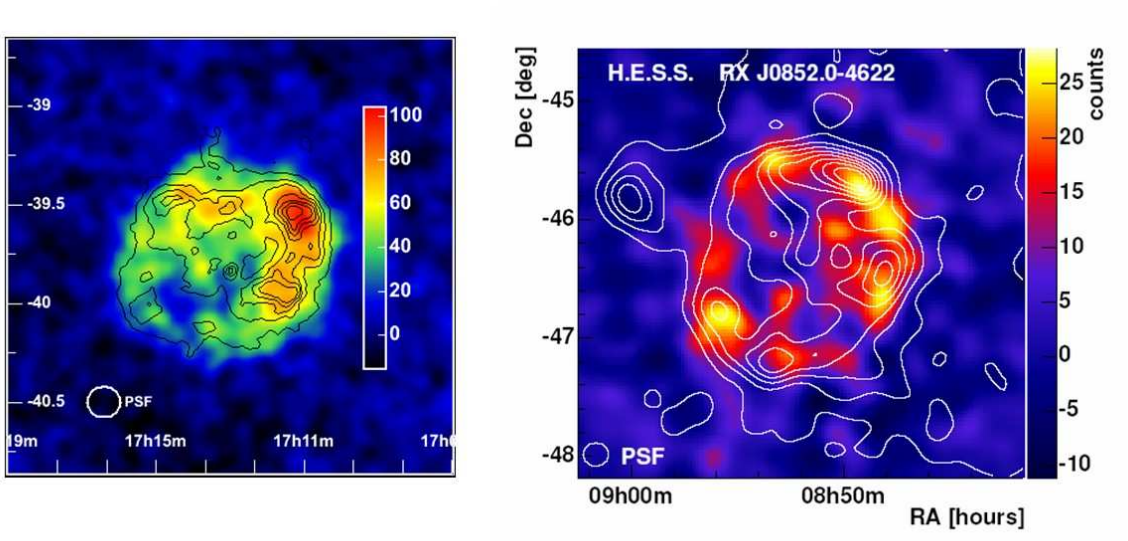

Figure 5. Supernova remnants RX J1713.7-3946 (left) and RX J0852.0-4622 ("Vela Junior", right). Color scale indicates gamma-ray count rates, contour lines the X-ray emission measured by ASCA (RX J1713-3946) [18] and ROSAT (RX J0852.0-4622) [19]

.

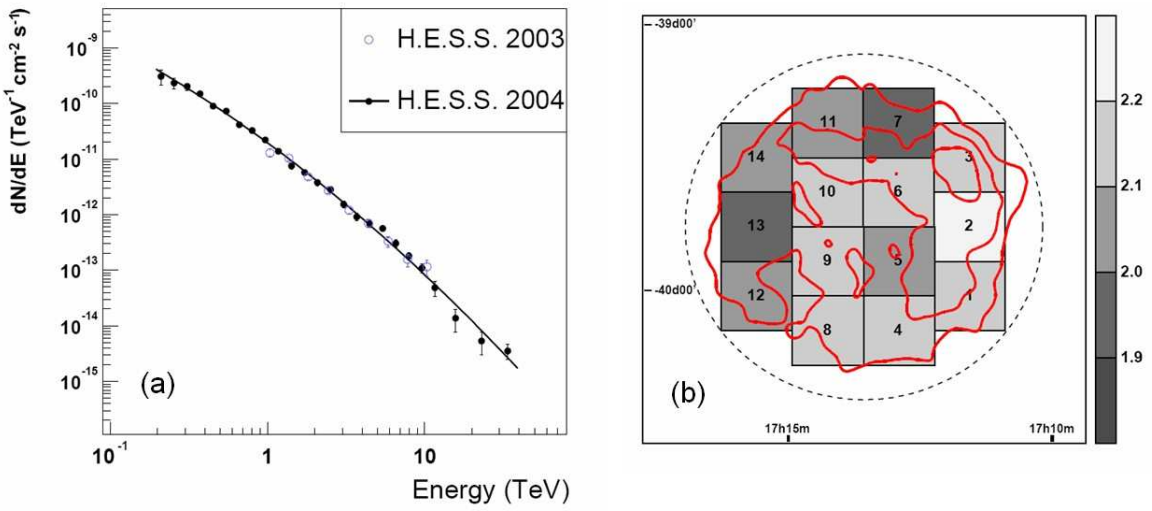

Figure 6. (a) Energy spectrum of gamma rays from RX 1713.7-3964, based on the 2003 data (open points) and the 2004 data (full points). (b) Spectral index determined from a power-law fit for 14 regions of the remnant. No significant variation of the index is found across the remnant. The contour lines indicate the gamma-ray flux.

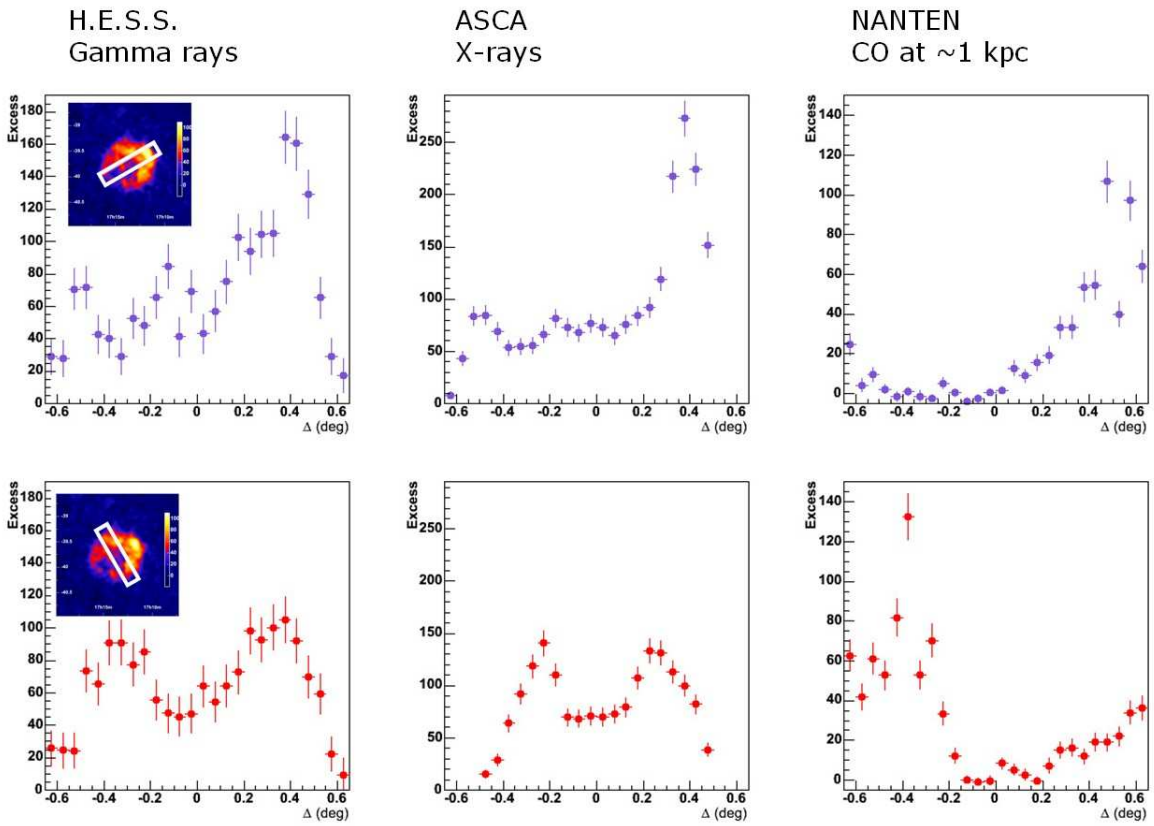

Figure 7. Slices across the remnant RX J1713.7-3946, in the direction from low to high gamma-ray intensity (top row) and in the orthogonal direction (bottom row). Left: rate of gamma rays; middle: rate of X-rays (ASCA [18]); right: CO intensity, measuring the density of interstellar clouds, in the velocity range corresponding to a distance around 1 kpc [20].

velocity selection corresponding to the suggested 1 kpc distance of the SNR, the molecular clouds, or parts thereof could be located before or behind the remnant. The orthogonal slice (bottom row) illustrates nicely the shell structure; for the correlation with X-rays (middle) and CO intensity (right), the same conclusions as for the first slice apply. However, simple electronic models fail to consistently fit the multiwavelength data (Fig. 8). From the relative levels of X-ray and gamma-ray intensities, a local magnetic field $B \approx 10\ \mu$G can be determined, assuming that X-rays represent synchrotron radiation ($\sim B^2$) and that the gamma rays are generated in Inverse Compton scattering. A standard E^{-2} electron injection spectrum describes the radio and X-ray spectra, but fails to account for the flat top of the gamma-ray spectrum; the Inverse Compton peak should be visible in the energy range covered by H.E.S.S. With a steeper spectrum, $E^{-2.5}$, the gamma-ray spectrum can be accommodated, but then model predictions overshoot the radio flux [21] by almost two orders of magnitude. In contrast, models which use a higher magnetic field (which suppresses the Inverse Compton component for a given X-ray intensity) and which add gamma-rays generated in proton interactions, achieve a good description of wide-band spectra, of course at the expense of introducing additional free parameters (proton flux and spectrum). In summary, remarkable progress has been made in pinning down SNRs as cosmic

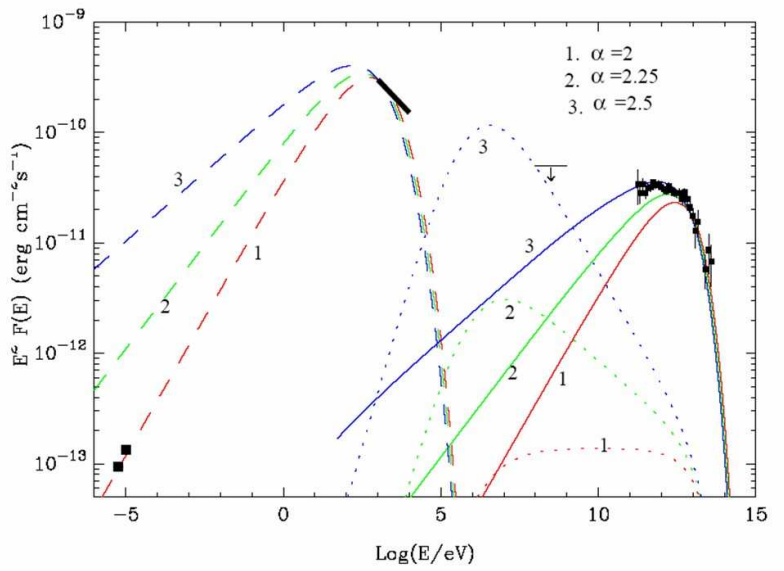

Figure 8. Wideband spectra of synchrotron radiation (dashed), bremsstrahlung (dotted, for a density of 1/cm^3) and Inverse Compton radiation (full lines), for a magnetic field around 10 μG and an electron injection index of 2.0, 2.25 and 2.5. Also shown are the TeV (H.E.S.S.), X-ray (ASCA) and radio data [21].

accelerators, and there is a preference for a hadronic origin of the high-energy gamma rays; however, fully conclusive evidence is still lacking.

4. H.E.S.S. observations of pulsar wind nebulae

Another interesting class of new TeV gamma-ray sources are pulsar wind nebulae (PWN), which are potentially responsible for a significant fraction of the new sources, and for some of the strongest [22]. A supernova explosion frequently leaves a pulsar behind, which, with it its high magnetic and electric fields, generates a steady stream of high-energy electrons and positrons. This pulsar wind blows a hole into the remnant, compressing ejecta in a pulsar wind termination shock, in which the electrons can be re-accelerated. The energy content of the pulsar wind is typically a few orders of magnitude lower than the kinetic energy available for particle acceleration in the supernova ejecta, which makes it surprising that pulsar wind nebulae - with the Crab Nebula as the best-studied example - are such prominent sources. The reason is that energy in pulsar wind electrons is far more efficiently converted to gamma rays than the energy of protons and nuclei accelerated in the main supernova shock. Typical radiative life times for electrons are O($10^3 - 10^4$) y, compared to O(10^7) y for protons, which compensates for the deficit in energy. PWN detected in X-rays sometimes appear shifted relative to the pulsar [23, 24]; explanations include a (single-sided) jet-like emission or the "crushing" of one side of the PWN by the reverse shock [25], which is released when the supernova shock wave has swept up a significant amount of material, generating a back-reaction. If a supernova explodes into an inhomogeneous environment - as most supernovae do - the reverse shock from the side of the denser medium will reach and crush the corresponding side of the PWN while - if observed at the right time - the other half of the PWN is still unaffected.

H.E.S.S. has detected a number of extended PWN, the most recent one is Vela X, associated with the Vela pulsar. Fig. 9 shows the intensity distribution of gamma rays, together with the ROSAT X-ray contours [23].

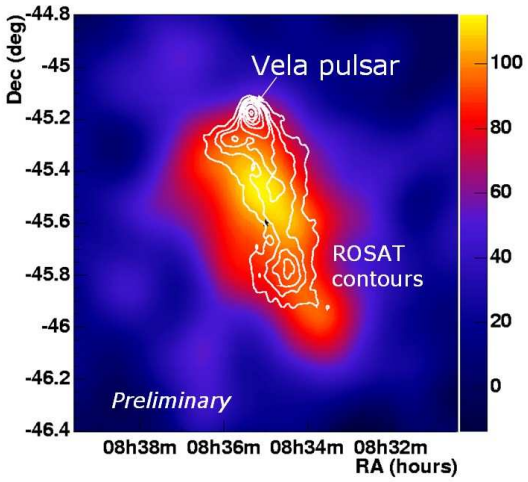

Figure 9. Smoothed map of VHE gamma-ray excess counts in the region of the Vela pulsar (colors), together with ROSAT X-ray contour lines (white). No significant gamma-ray excess is detected from the pulsar itself.

The gamma ray source extends almost a degree south of the pulsar, and features a very hard energy spectrum reaching up to 50 TeV, with a photon index of 1.9. The spectrum is clearly curved; a better fit than with a simple power law is obtained with a power law with high-energy cutoff. At the location of the Vela pulsar itself, no significant steady or pulsed emission is detected.

Another interesting PWN is MSH 15-52, associated with the pulsar PSR B1509-58 inside the G 320.4-1.0 / RCW 89 shell. The elongated and single-sided nebula was seen in ROSAT images [26]; high-resolution Chandra images [27] revealed a jet-like feature. MSH 15-52 was first detected as a gamma-ray source by CANGAROO [28]. H.E.S.S. observations resolve an extended source [29] (Fig. 10(a)), aligned in the same direction as the Chandra jet feature, and with a power-law energy spectrum extending to well beyond 10 TeV (Fig. 10(b)).

A particularly nice candidate for a displaced PWN is HESS J1825-137. Located south of the pulsar PSR B1823-13, the VHE gamma-ray emission peaks at the pulsar and then falls off towards the south (Fig. 11). Exactly the same feature is seen in X-rays [30], except that the characteristic extension of the nebula is a few arcminutes rather than a fraction of a degree. A natural explanation is [31] that in the estimated 10 μG field in the nebula, the X-ray generating electrons have higher energies than those responsible via Inverse Compton scattering for the VHE gamma rays. The higher-energy X-ray electrons cool faster and have a shorted range.

5. Binary systems studied with H.E.S.S.

Binary systems consisting of a compact object orbiting a massive star have frequently been suggested as VHE gamma-ray emitters; their often eccentric orbits allow the study of how gamma-ray emission varies with the distance between pulsar and the companion star. PSR B1259-63 is a distant binary, consisting of a pulsar in

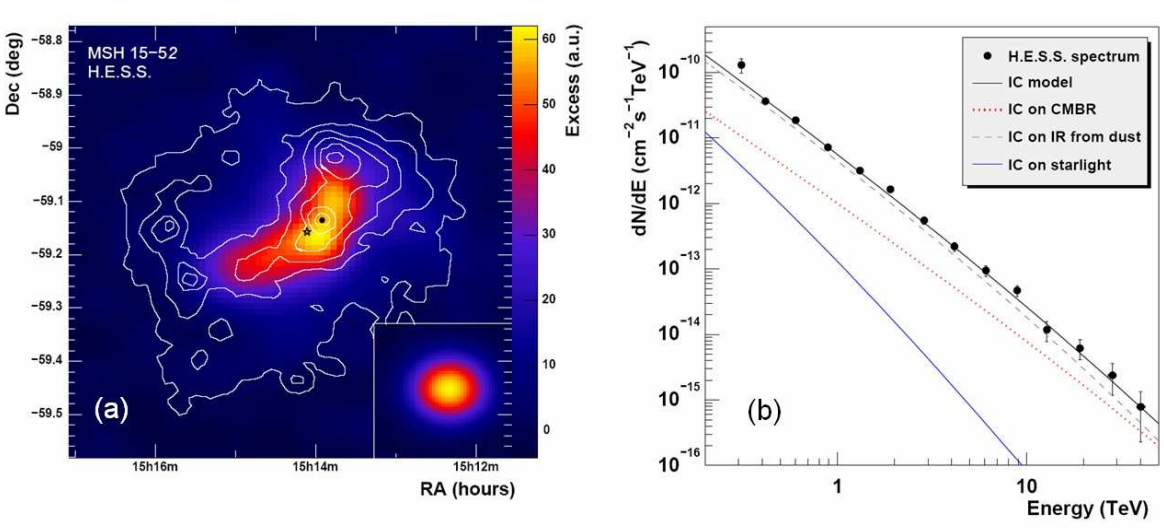

Figure 10. (a) Smoothed excess map from MSH 15-52 [29]. The white contour lines denote the X-ray count rate measured by ROSAT [26]. The black point and the star lie at the pulsar position and at the excess centroid, respectively. The inset shows the point spread function after smoothing. (b) Gamma-ray spectrum from MSH 15-52. The lines show the result of a fit to X-ray and gamma-ray spectra, where gamma rays result from Inverse Compton upscattering by electrons, with microwave background, IR from dust and starlight as targets [29].

a highly eccentric 3.4 y orbit around a massive star with a disk-like equatorial wind. The closest approach - last in March 2004 - is about 20 stellar radii. Near periastron, particles potentially accelerated by the pulsar find enhanced targets for generating gamma-rays, both in the form of the intense photon field of the star, and in the form of the stellar wind. In February 2004, H.E.S.S. detected this system as a TeV source [32] (Fig. 12). Surprisingly, however, the light curve - interrupted by full-moon periods - indicates a double-humped shape with a minimum near periastron. This time variation suggests that interactions of the pulsar wind with the disk-like stellar wind dominate the shape of the light curve. Another surprise was the discovery of a second, steady and extended ($0.16°$) gamma-ray source about $0.5°$ north of the pulsar, HESS J1303-631 [33]. HESS J1303-631 – with a spectrum with photon index $\Gamma \approx 2.4$, reaching up to 10 TeV – is another "dark accelerator" without known counterpart at other wavelengths, despite of follow-up observations with Chandra [34].

A source discovered in the Galactic plane survey, HESS J1826-148 (Fig. 13(a)) [7], is coincident with a close binary, LS 5039, consisting of a few-solar-mass compact object in a 4 day orbit around a massive star, with a closest approach around 2 stellar radii. The compact object accretes mass from the massive star; the system is particularly remarkable in that VLA radio observations [35] have revealed the existence of two jets, making this a "microquasar" in close analogy to active galaxies, except that mass and time scales are reduced. More recent data provide enhanced significance for this source (Fig. 13(b)) [36]. For this first microquasar discovered as TeV emitter, H.E.S.S. finds a relatively hard spectrum, resulting in a seemingly continuous emission spectrum across nearly all wavelength ranges (provided that the EGRET source 3EG J1824-1514 is actually associated with LS 5039; the large position errors make a clear assignment difficult) (Fig. 13(c)).

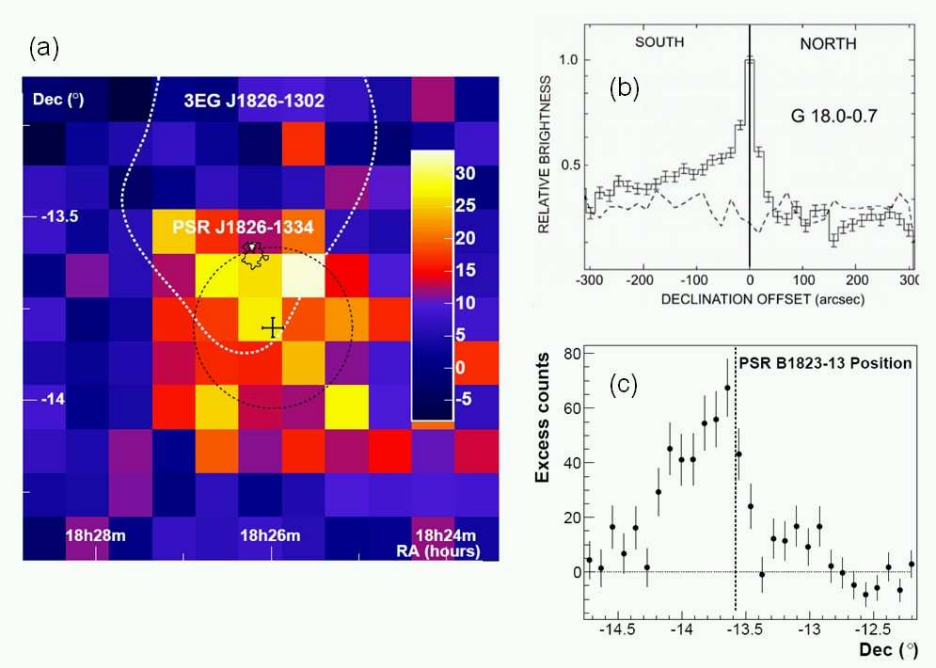

Figure 11. (a) Distribution of gamma-ray excess counts for HESS J1825-137, near the pulsar PSR B1823-13 (= PSR J1826-1334). (b) X-ray [30] and (c) gamma-ray counts in a slice in declination, centered on the pulsar.

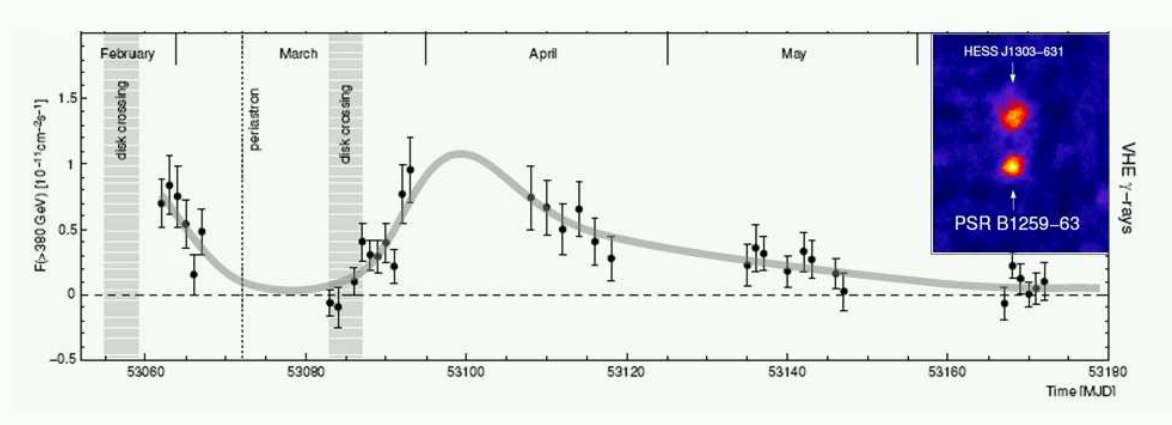

Figure 12. Light curve of VHE gamma rays from the direction of the pulsar PSR B1259-63. The dotted line indicates the point of closest approach between the pulsar and the Be star, the shaded areas show the (approximate) crossing of the disk-like stellar wind. The small inset shows the field around PSR B1269-63 as seen in February 2004, with the second source HESS J1303-631 north of the pulsar.

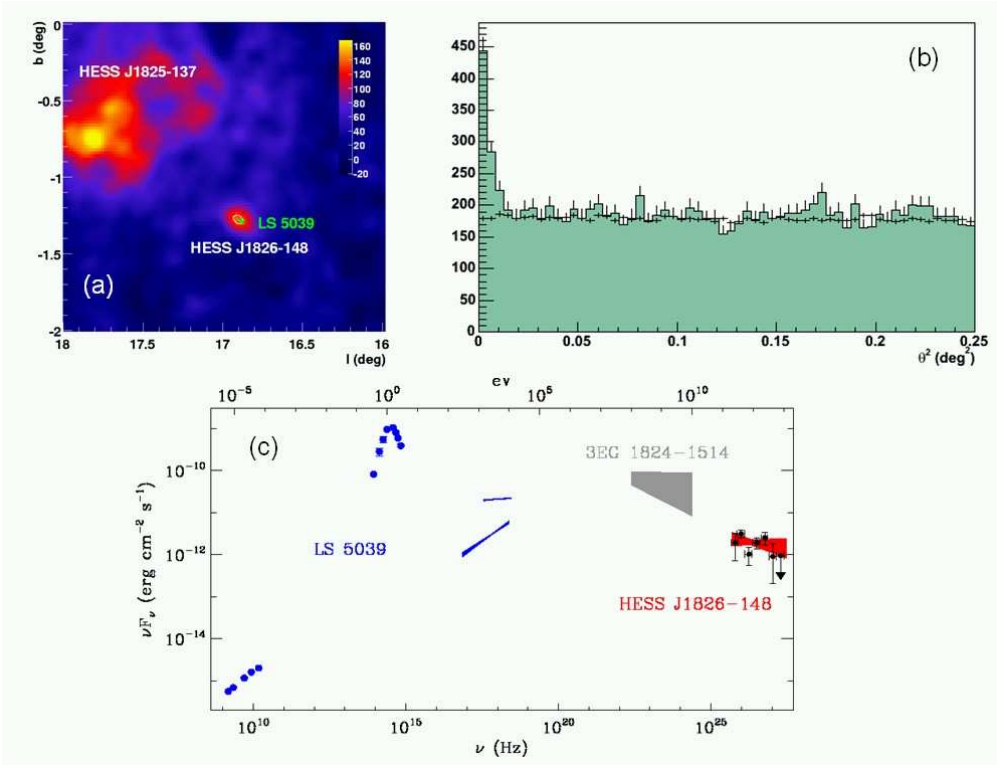

Figure 13. (a) Map of gamma-ray emission for the region around LS 5039 based on the 2004 data set, showing the extended source HESS J1825-137 and the point-like source HESS J1826-148, coincident with LS 5039 [7]. (b) Angular distribution relative to the source position for HESS J1826-148, including more recent additional data, resulting in a significance of 16 σ. (c) Wide-band spectral energy distribution of LS 5039, assuming that both 3EG 1824-1514 and HESS J1826-148 are related to LS 5039 [7].

6. H.E.S.S. observations of the Galactic center region

Another very interesting region is obviously the Galactic center. H.E.S.S. detected two sources near the Galactic center, HESS J1747-281 [37], coincident with the SNR G0.9+0.1 and HESS J1745-290 [38], coincident with the Sgr A complex (see also Fig. 15(a)). The source of gamma rays in SNR G0.9+0.1 is presumably again a PWN; the gamma ray source is definitely smaller than the SNR shell visible in radio [37]. The origin of the source at the Galactic center – prior to H.E.S.S. seen by CANGAROO [39] and VERITAS [40] with lower significance – is less clear; it could be associated with processes near the central black hole, with the SNR Sgra A East or with the annihilation of speculative dark-matter particles ("neutralinos") left over from the big bang and responsible for structure formation in the universe; the density of such particles should peak as $r^{-\alpha}$ at the Galactic center, with $\alpha \geq 1$ derived from many-body simulations. The location of the H.E.S.S. source is within the 20" systematic pointing errors fully consistent with Sgr A*, but an origin in Sgr A East cannot safely be excluded. A possible clue could therefore come from the exact angular distribution of the gamma rays (Fig. 14(a)). Indeed, while the peak at small angular distance from Sgr A* is essentially consistent with the angular resolution of the instrument, the angular distribution has a pronounced tail, which is not accounted for by the point spread function. A fit based on dark-matter distributions yields good agreement for $\alpha \approx 1.0$.

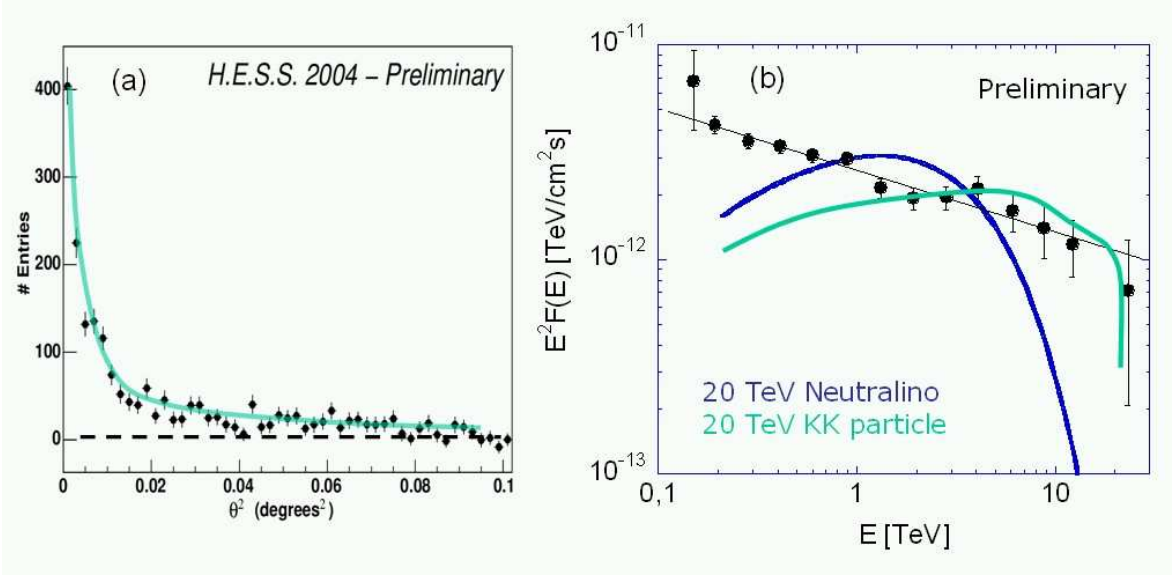

Figure 14. (a) Angular distribution of the gamma-ray emission from the Sgr A source HESS J1745-290. Shown is the distribution in the angle θ^2 relative to the source. (b) Spectral energy density of HESS J1745-290. Lines: spectra resulting from the annihilation of typical MSSM neutralinos and from Kaluza-Klein dark-matter particles [43].

More constraints concerning the nature of the source can come from the spectrum and the time variability of the flux. The measured spectrum Fig. 14(b)) [41] is a pure power law, extending, with the most recent H.E.S.S. data, over two decades in energy. The measured flux is consistent with constant emission, on scales of (2) years, months, days and hours. However, caveats to be listed are that the total integrated observation time in 2003/4 was about 40 h, so flares might have been missed. Also, short flares (on daily or hourly time scales) must have a significant amplitude (flux variations of factors of a few) to be detectable. Nevertheless, the steady emission disfavors processes in the immediate vicinity of the black hole Sgr A*. Concerning the dark-matter signature, the observed power law spectrum does not match the typical (quark or gluon-fragmentation type) gamma-ray spectra from neutralino annihilation [42] (Fig. 14(b)), even ignoring the fact that most models prefer neutralinos in the energy range up to 1 TeV, not capable of generating spectra which extend beyond 10 TeV. Classical SUSY neutralinos have strongly curved spectra, at variance with observations. Models based on Kaluza-Klein dark matter particles provide enhanced few-body decay modes and flatter spectra [43], and are capable of reproducing the early H.E.S.S. 2003 data set. The full 2004 spectrum, extending down to 150 GeV, is not reproduced by these models [44] (Fig. 14(b)). Hence, it seems very improbable that the full gamma ray signal from the Galactic center is caused by dark matter annihilation. A partial contribution, in particular at low energies, cannot be excluded.

The extended component of gamma-ray emission in the Sgr A region could also be related to diffuse emission of cosmic rays interacting with the dense molecular clouds in this region; the resulting gamma rays flux should be detectable with H.E.S.S. Indeed, subtracting the two point sources HESS J1745-290 and HESS J1747-281 leaves a clear excess extending along the Galactic ridge, between $-1°$ and $1°$ longitude, and a (rms) width of about $0.2°$ in latitude (Fig. 15(b)) [45]. Apart from a region at $l \approx 1.5°$, the excess traces the density of molecular clouds estimated via their CS emission [46] (Fig. 15(c)). The spectrum of the diffuse component (Fig. 15(d)) is similar to the spectrum observed for the central source HESS J1745-290, and has a spectral

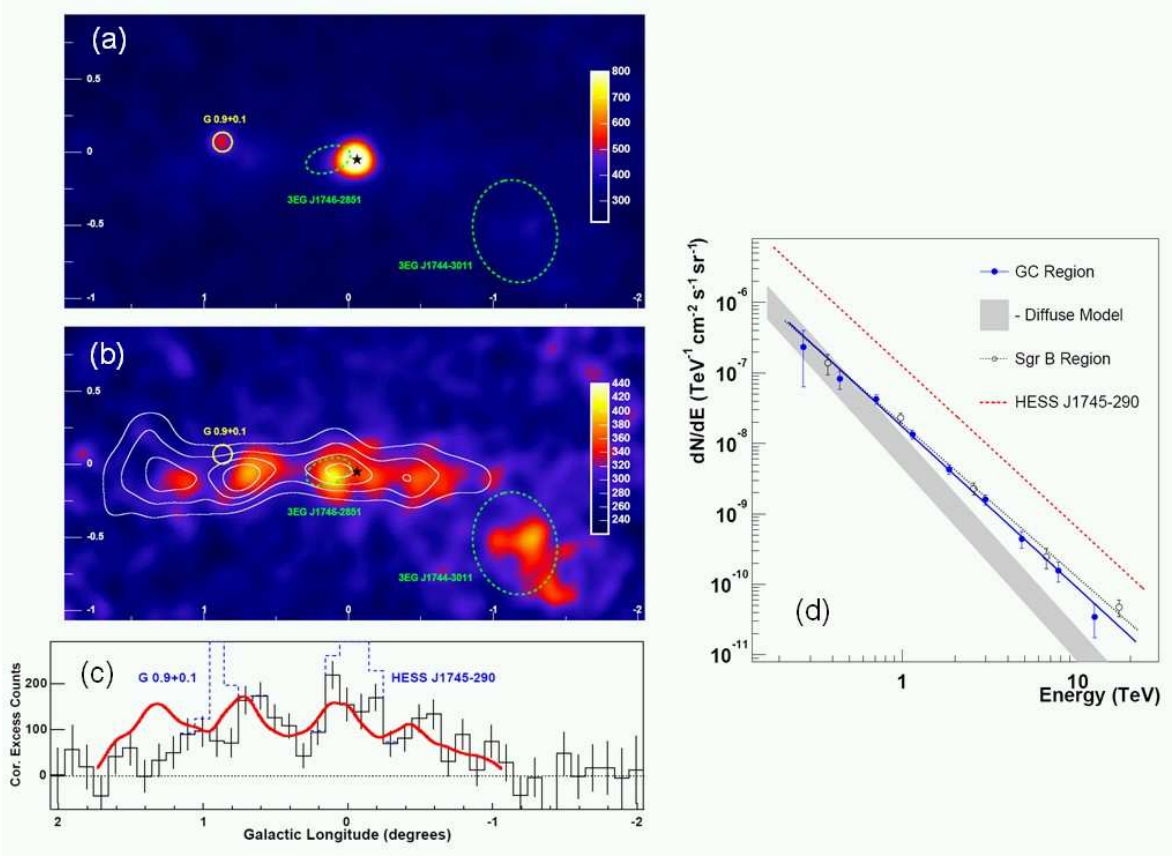

Figure 15. (a) Gamma-ray sky map of the Galactic center region, showing the supernova remnant G0.9+0.1 and Sgr A as prominent sources. (b) Sky map after subtraction of point sources at the locations of G0.9+0.1 and Sgr A, revealing a band of diffuse gamma-ray emission. White contours indicate the density of molecular gas, traced by its CS emission [46]. (c) Slice along Galactic longitude, showing the diffuse gamma-ray excess after subtraction of the point sources (which are shown as dashed lines). The red curve shows the density of molecular gas, traced by the CS emission. (d) Spectrum of the diffuse emission from the entire band (full points) and from the Sgr B region (open points), compared to the emission from the Sgr A point source (dotted line) and the expected diffuse emission assuming the cosmic ray flux measured on Earth (shaded band). All data shown are preliminary.

index of 2.3, harder than expected for gamma rays from interactions of cosmic rays with the spectrum locally measured on Earth, and showing an excess over the such predicted spectrum at higher energies. Given the proximity of accelerators and targets in the complex region near the Galactic center, a harder spectrum is expected since effects of diffusion and escape should be reduced. An open question remains the deficit of emission - compared to the density of molecular clouds - around $l \approx 1.5°$. One speculative explanation is that the cosmic rays interacting with the clouds were “recently” (some 10000 years ago) generated by an accelerator near $l = 0$ and did not yet have sufficient time to diffuse beyond $|l| = 1°$. An alternative explanation for the diffuse gamma-ray band is provided by assuming a superposition of O(10) point-like sources, with a distribution governed by that of the molecular gas.

7. Extragalactic sources detected by H.E.S.S.

Turning now to extragalactic sources, two new H.E.S.S.-discovered distant blazars [47] are of particular interest for the estimates of the extragalactic background light (EBL). The EBL filling extragalactic space has been accumulated since the first galaxies were formed and contains cosmological information about the history and evolution of galaxies and early stars. VHE gamma rays interact with EBL photons by electron-positron pair production, resulting in an energy dependent attenuation of the gamma rays (e.g. [48, 49]). Since the interaction cross section peaks near pair production threshold, there is an approximate correlation between gamma ray energy and EBL photon frequency. Gamma ray spectra contain encoded in their attenuation features the EBL spectrum; however, since the intrinsic spectrum at the source, before attenuation, cannot (yet) be predicted, one can mainly derive upper limits on the EBL from gamma-ray observations of distant AGN: high EBL levels will – for typical EBL spectra – result in a strong steepening of gamma-ray spectra, requiring unphysical spectra at the source in order to reproduce the spectra measured on Earth.

H.E.S.S. has discovered two new distant blazars [47], 1ES 1101-232 [50] at a redshift of 0.186 and H2356-309 [51] at a redshift of 0.165, both with good statistical significance (Fig. 16(a)). Both objects were selected as observation targets on the basis of their high radio and X-ray flux [52]. Both exhibit similar spectra, with a

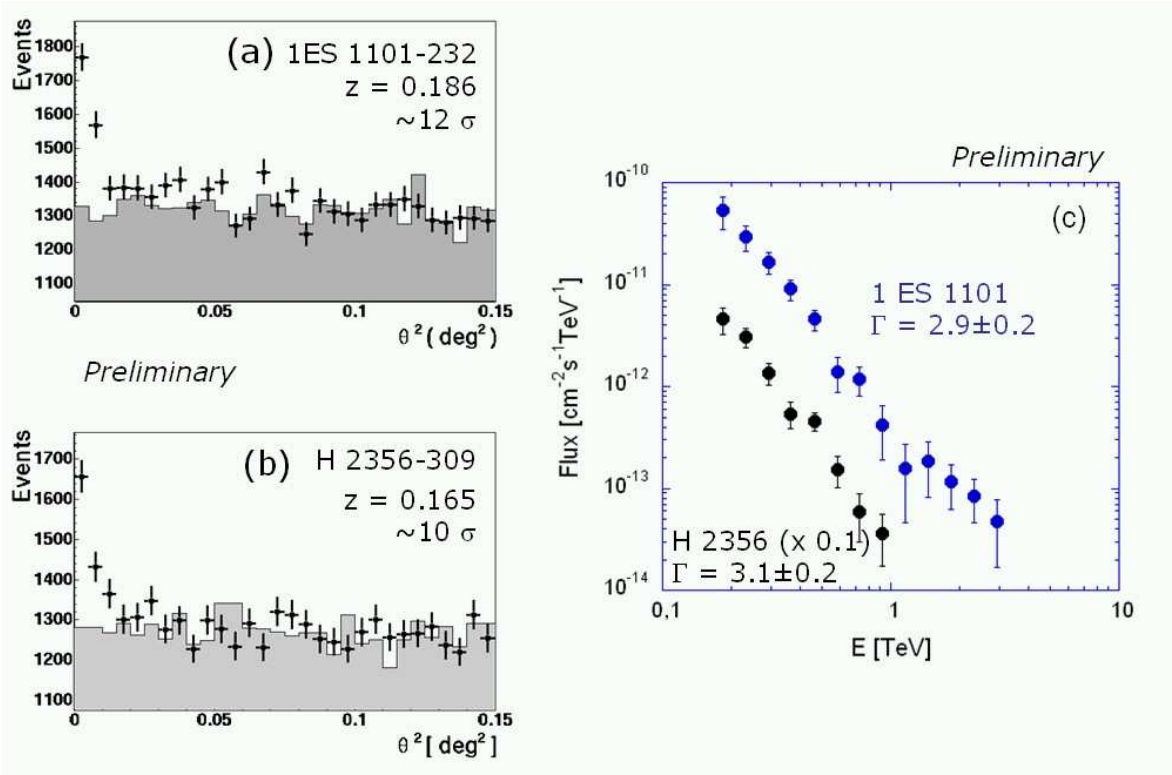

Figure 16. (a) Angular distribution of gamma ray candidates relative to the positions of 1ES 1101-232 (a) and H2356-309 (b); the background estimates are shown as grey areas. (c) Energy spectra measured for the two sources [47].

photon index of 2.9 ± 0.2 for 1ES 1101-232 and of 3.1 ± 0.2 for H2356-309 (Fig. 16(b)). To obtain limits

on the EBL, is it assumed that intrinsic source spectra have a photon index of $\Gamma = 1.5$ or larger (defined via $\mathrm{d}N/\mathrm{d}E \sim E^{-\Gamma}$); this represents the smallest index obtained for conventional acceleration models followed by gamma-ray production via the Inverse Compton process. For the EBL, a reference shape is assumed [53] (Fig. 17), optionally augmented by a near-infrared bump as suggested by some measurements [54]. The EBL is level is then varied by scaling factors. The result [47] is that only EBL shapes at a level below 0.55 of the reference shape generate acceptable source spectra; the near-infrared bump is clearly ruled out. For example, the reference EBL level would require an intrinsic spectral index for 1ES 1101-232 of $\Gamma = -0.1$; the additional near-infrared component would require $\Gamma = -0.9$. The new upper limit on EBL intensity is within 30% from the lower limit obtained from galaxy counts [55], indicating that (a) the EBL sources are largely resolved and (b) that the universe is more transparent for VHE gamma rays than previously thought.

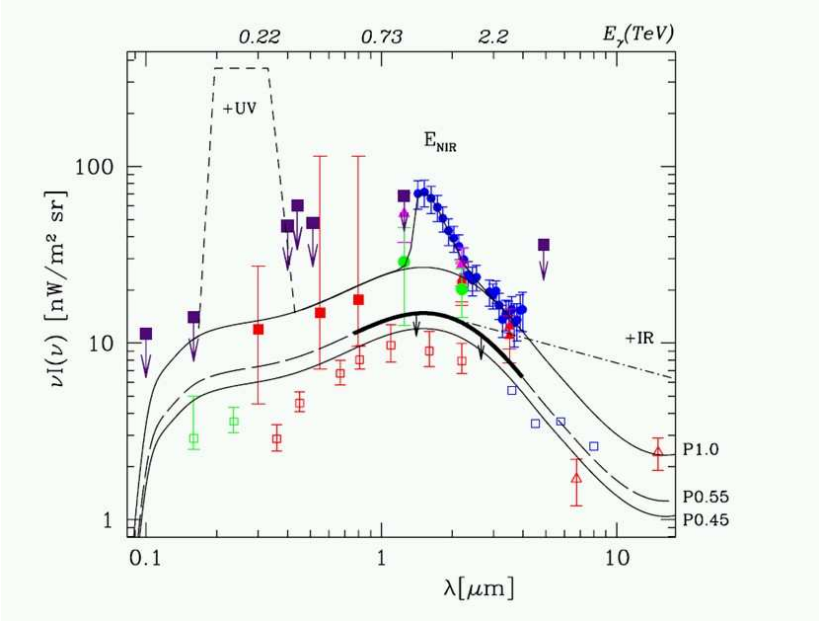

Figure 17. Spectral energy distribution of the extragalactic background light (EBL) from 0.1 to 20 μm [47]. Open symbols refer to the integrated light from galaxy counts and have to be considered as lower limits. The full line (P1.0) gives a reference shape for the EBL intensity; E_{NIR} denotes an additional contribution in the near infrared claimed to the basis of IRTS data [54], possibly caused by Population III stars. The line P0.55 represents the maximum EBL level consistent with the gamma-ray spectra of 1ES 1101-232 and H2356-309, and constrains the EBL in particular in the 1-3 μm region.

In summary, the first results from H.E.S.S. have revealed a number of interesting new objects in the TeV sky – among them many extended sources – providing a new handle to study processes in the sources. The H.E.S.S. results also demonstrate that Cherenkov instruments of the latest generation have passed a critical sensitivity threshold, where real VHE gamma-ray astronomy becomes feasible.

Acknowledgements

This report represents the cumulative effort by the H.E.S.S. collaboration in building and operating the instrument and in analyzing the data. The author would like to emphasize in particular the key contributions by many of our outstanding students and postdocs, who deserve the lion's share of the credit for the success of the H.E.S.S. project.

References

[1] K. Bernlöhr et al., Astropart. Phys. 20 (2003) 111.
[2] P. Vincent et al., 2003, in Proc. 28th ICRC, Tsukuba (Univ. Academy Press, Tokyo), 2887.
[3] W. Hofmann, "H.E.S.S. Status", Proc. of the Cherenkov 2005 workshop, Palaiseau, France (to be published).
[4] F.A. Aharonian et al., Science 307 (2005) 1938.
[5] F.A. Aharonian et al., astro-ph/0510397, ApJ, in press.
[6] S. Funk and A. Lemiere, Proc. 29th ICRC, Pune, 4, 123 (2005).
[7] F.A. Aharonian et al., Science 309 (2005) 746.
[8] R.L. White, R.H. Becker, D.J. Helfand, AJ 130 (2005) 586.
[9] C.L. Brogan et al., ApJ 629 (2005) L105.
[10] D.J. Helfand, R.H. Becker, R.L. White, astro-ph/0505392 (2005).
[11] P. Ubertini et al., ApJ 629 (2005) L109.
[12] F.A. Aharonian et al., Nature 307 (2005) 1938.
[13] D. Berge, Proc. 29th ICRC, Pune, 4, 117 (2005).
[14] F.A. Aharonian et al., A&A 437 (2005) L7.
[15] N. Komin, 29th ICRC, Pune, 4, 135 (2005).
[16] H. Muraishi et al., A&A 354 (2000) L57.
[17] H. Katagiri et al., ApJ 619 (2005) L163.
[18] Y. Uchiyama et al., AIP Conf. Proc. 745, p. 305 (2005).
[19] Voges et al., A&A 349 (1999) 389.
[20] Y. Fukui et al., PASJ 55 (2003) L61.
[21] J.S. Lazendic et al., ApJ 602 (2004) 271.
[22] B. Khelifi, 29th ICRC, Pune, 4, 127 (2005).
[23] C.B. Markwardt, H.B. Ögelmann, ApJ 480 (1997) L13.
[24] B.M. Gaensler et al., ApJ 588 (2003) 441.
[25] J.M. Blondin, R.A. Chevalier, D.M. Frierson, ApJ 563 (2001) 806.
[26] E. Trussoni et al., A&A 306 (1996) 581.
[27] B.M. Gaensler et al., ApJ 569 (2002) 878.
[28] T. Sako et al., ApJ 537 (2000) 422.
[29] F.A. Aharonian et al., A&A 435 (2005) L17.
[30] B.M Gaensler et al., ApJ 588 (2003) 441.
[31] F.A. Aharonian et al., astro-ph/0510394, A&A, in press.
[32] F.A. Aharonian et al., astro-ph/0506280 (2005), A&A, in press.
[33] F.A. Aharonian et al., A&A 439 (2005) 1013.
[34] R. Mukherjee, J.P. Halpern, ApJ 629 (2005) 1017.
[35] J.M. Paredes et al., Science 288 (2000) 2340.
[36] M. de Naurois, 29th ICRC, Pune, 4, 101 (2005).
[37] F.A. Aharonian et al., A&A 432 (2005) L25.

[38] F.A. Aharonian et al., A&A 425 (2004) L13.
[39] K. Tsuchiya et al., ApJ 606 (2004) L115.
[40] K. Kosack et al., ApJ 608 (2004) L97.
[41] L. Rolland, 29th ICRC, Pune, 4, 109 (2005).
[42] P. Gondolo et al., 2004, http://www.physto.se/ edsjo/darksusy/.
[43] L. Bergstrom et al., Phys. Rev. Lett. 94 (2005) 131301.
[44] J. Ripken, 29th ICRC, Pune, 4, 151 (2005).
[45] J. Hinton, 29th ICRC, Pune, 4, 21 (2005).
[46] M. Tsuboi, H. Toshihiro, N. Ukita, ApJSS 120 (1999) 1.
[47] F.A. Aharonian et al., astro-ph/0508073 (2005).
[48] R.J. Gould, G.P. Schreder, Phys. Rev. Lett. 16 (1966) 252.
[49] F.W. Stecker, O.C. de Jager, M.H. Salamon, ApJL 390 91992) 49.
[50] S. Pita, 29th ICRC, Pune, 4, 287 (2005).
[51] M. Tluczykont, 29th ICRC, Pune, 4, 291 (2005).
[52] L. Costamante, L. Ghisellini, A&A 384 (2002) 56.
[53] F.A. Aharonian et al., A&A 403 (2003) 523.
[54] T. Matsumoto et al., ApJ 626 (2005) 31.
[55] P. Madau, L. Pozzetti, MNRAS 312L (2000) 9.